Scanning Near-shore Intertidal Terrain Using Ground LiDAR

Chien-Ting Wu[1]* Ming-Cheng Chen[2] Cheng-Yang Hsiao[3]

ABSTRACT Intertidal zone refers to the area under and above the water during high and low tides. Traditionally, this zone is not within the scope of land management authorities. Moreover, in accordance with principals set out by existing plans, intertidal zones are excluded from management zones. Boundaries should therefore be set at the land and sea border. Traditionally, methods in determining this have included the traditional theodolite (total station) method, mapping and aerial photography (photogrammetry). However, existing operational restrictions lower efficiency, in addition to increasing time and operational costs. Therefore this paper explores the practicality of a user-friendly, ground-based high resolution laser scanning technology. This method offers easy operation and high-density characteristics with an instrument platform that can be installed on elevated rooftops. High accuracy and resolution is achieved using a stop-and-go method producing Digital Terrain Model (DTM) data. The range of the completed data is 61km in length, 2.5km in width, and -0.5m depth, with a sampling error of approximately ±2cm. Through the implementation discussed in this research, accurate information about the changes of topography in intertidal areas can be obtained.

Key Words : LiDAR, Laser, Intertidal Area Topography.

I. Introduction

Due to the intertidal topography between the land and ocean borders, effects on both can be observed. The effects from both the land and ocean create special landscapes with unique topography and ecology. Changes in the marine or terrestrial environment can therefore directly or indirectly affect the intertidal zone. Monitoring intertidal changes assist in the controlling of groundwater, land subsidence and coastal erosion which better protects the marine environment and strengthens coastal management.

The mapping of the intertidal zone can be divided into two parts – the ocean and terrestrial zones. In terms of undertaking intertidal surveying work within the water, the depth sounder (fathometer) is used for water depth measurements. Measurements within this area are taken at the lowest point of 5m in addition to sonar measurements taken via aerial methods (involving aerial route planning). Environmental and operational constraints are present when measuring the equivalent area on land. This reduces efficiency and increases operating time and costs. Another constraint is low tidal events and the presence of obstacles causing measurements to become inconvenient. Recent years have seen the development of new laser scanning technology such as the Bathymetric LiDAR. This method calculates depth by using a green laser system and a near-infrared light. While the near-infrared light will reflect off the surface of the sea, the green laser will penetrate the surface and reflect off the sea-bed. The depth is determined by the time differences between the reflections of two beams. Though the LiDAR system can rapidly measure a wide range of area, shortcomings are still present such as the lack of resolution and precision when there is a lack of lighting. These operations also require abidance to flight routes and aircraft schedules, involve high operational costs, specialized software, human resources in post-operation data processing and so forth. Therefore this research uses two ground based laser systems combined with real-time VBS-RTK location confirmation systems. Tidal changes within a two week timeframe were recorded within a 61km span of coastline, with the resultant data used in 3D scanning.

II. Literature Review

Due to measurement restrictions in shallow waters typically observed at the land-ocean boundary, a zone exists where it is difficult to undertake measurements. To overcome this problem, a specialized calculation method may be applied. This concept was brought about by a French mathematical geologist named Kriging (Matheron 1963). By using the theory of regionalized space variables, the distribution of the natural topography can be investigated. Accurate estimates of the changes in the topography of the region can then be undertaken (Fang et al. 2006). Measurements can be measured at an elevation of -1m to +1m, within -1.5m to 1.5m and -2m to 2m of space. The average sampling error is approximately 0.039m, 0.163m and 0.237m.

With the development of the laser scanning technology comes many new applications with this technology. For example Aerial LiDAR uses flight routes and multilayer scanning in achieving DSM and DEM (Wang et al. 2005). However to achieve Aerial LiDAR, extensive planning and knowledge in

〔1〕國立交通大學土木工程研究所
Department of Civil Engineering, National Chiao Tung University, Hsinchu, Taiwan, R.O.C.
〔2〕健行科技大學空間資訊與防災工程研究所
Department of Geoinformatics and Disaster Reduction Technology, Ching Yun University, Chung-Li, Taiwan.
〔3〕中興工程顧問社防災科技研究中心
Disaster Prevention Technology Research Center, Sinotech Engineering Consultants, Inc.
* Corresponding Author. E-mail : kenwu@uch.edu.tw

flight planning, the range of the scanning area, geographical terrain,, and scanning angle range is required. Each route must take into account the ground width, flight route overlapping, route crossover locations, cloud point density, tidal information, and air traffic information. As a result, undertaking this task requires more than merely generating a flight plan. As such, more information and planning is required for the feasibility for this aerial survey. Ground based laser systems are easy to operate, mobile and the scope of operation includes scanning historic relics, bridge structures, construction monitoring, suspension bridges monitoring (Chen et al. 2010) and slope monitoring. The emitted laser of the ground-based laser system is absorbed by water (it cannot penetrate the water, except for shallower waters) (Smart et al. 2009). Therefore, to increase the chances of obtaining the optimal results, the tidal status of the intertidal region should be considered.

In 2007, an e-GPS satellite was deployed for the Taiwanese region. The Global Position Satellite (GPS) system, along with a Virtual Base System (VBS) and the dynamic position technology (RTK) has a horizontal accuracy or error of less than or equal to 2cm, with a vertical accuracy or error of less than or equal to 5cm (Wang et al. 2006). This positioning accuracy is already widely used. Therefore this research focuses on VBS-RTK ground based real-time control point laser system.

III. Research Methods

1. Summary description of the scanning range

This research focuses on the scanning range between the coast of Zhānghuà Wu River (Tatu River) to Zhuóshuǐ River within the scope of the intertidal zone including terrain and surrounding structures (e.g. seawalls and roads). A full map including the scanned area is shown in Figure 1. Due to the high altitude mountains with rapid river flows within the Zhuóshuǐ Wu River and the Da Jia River, they are affected by drifting sands (longshore drift). This forms alluvial plains with level beach slops (about 1/1000). At low tide, the tidal width is approximately 5km, as shown in figure 2(b). The level of the beach slope has also increased over time, with the evidence of the low tide gradually retracted. Developments in this area have included a large number of fish farms and ponds for aqua-agriculture purposes consuming large amounts of fresh water. This ground water has a constant temperature with low costs in developing from these resources. However, extraction of this groundwater on a large scale causes land subsidence in parts of the extraction site.

2. Operating procedure

The tested area had a length of up to 61km. Before any laser scanning and testing of this area an on-site reconnaissance of the tested area was required, including understanding the structural and geographical characteristics of the area. After a detailed topographic survey was completed, this research selected a medium scan range (up to 300m) and long scan range (up to 2,500m), using two ground based laser systems (LiDAR) operating simultaneously. Therefore, this assisted in the selection of the ideal scanning locations along the coastline.

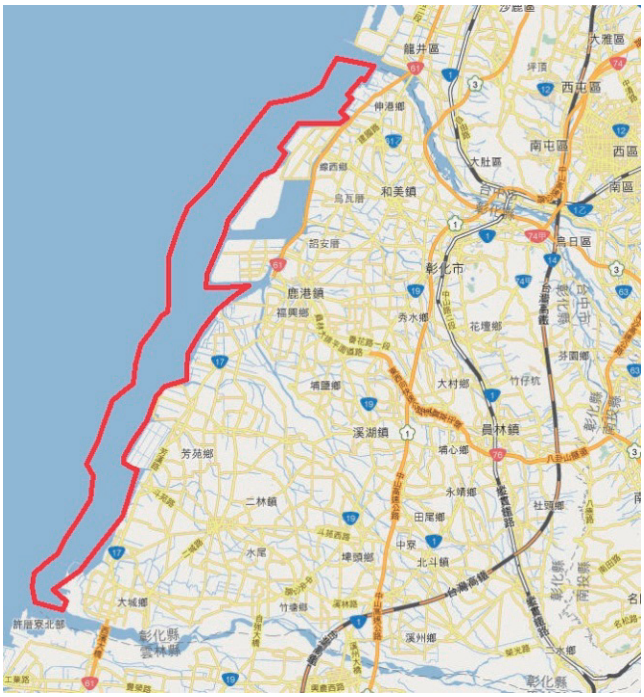

Fig.1 Studied coastal area within this research

Fig.2(a) High tides of the tested area

Fig.2(b) Drifting sands and deposition appearance of the tested area

The ground-based laser instrumentation uses a coordinate system which can only be adapted for use in Taiwan by the addition of measurement control points. Considering the vast range of the coastline and the distance between the control points, establishing the link between control points is difficult thereby increasing operating times. Therefore, this study uses VBS-RTK in the setup of temporary stations around 4-5 control points. By undertaking conversion work using coordinates obtained from the instrumentation and the actual coordinates, a data file with cloud points can be generated for use as coordinates in Taiwan. Post-processing of the cloud points includes filtering, segmenting and merging using the software package Trimble Realworks 4.22.

This study used two three-dimensional (3D) laser instrumentations (LiDAR). The Trimble GS2000 and the RIGEL DIBIT LPM 2K LiDAR systems were used. The performance specifications are outlines below in Table 1 and Table 2.

In order to accelerate the scanning process and increase mobility, a stop-and-go method was used whereby the 3D laser instrumentations were placed on the rooftop of a mobile platform. This allowed for the operator to quickly, safely, and conveniently move to different scanning locations. Upon reaching the fixed point, rapid real-time positioning of control point should occur.

In 2007, the national e-GPS system was completed in Taiwan, allowing for a benchmark measurement network. Using continuous observation of data, a regional interpolation positioning error mode can be constructed. In conjunction with virtual base stations and real-time dynamic positioning technology, the measured results with the checkpoints were compared with the original coordinates using VBS-RTK real-time measuring. The horizontal axis of the checkpoints had an average difference of up to 1.3m, with the vertical axis of the checkpoints having a difference of up to 1.3m (Chu and Chien 2004). The VBS-RTK used the Leica ATX-1230GG as the operating apparatus.

3. The ground-based LiDAR

The ground-based LiDAR (Light Detection And Ranging) is a remote 3D laser optical scanner. A 3-D laser scanner can record vast amounts of dimensional information on various surfaces in minimal time due to its capability to measure up to ten thousand points per second; the sheer amount of measurement data momentarily generated requires the connection to a computer for instantaneous data storage. It can rapidly locate numerous relative coordinate values and concretely describe the surface characteristics of targets.

3D laser scanners, use the principle of laser distance ranging and emit laser beams continuously, which reflect upon contacting the surface of objects. These signals are then received by the scanner. 3D laser scanners can extrapolate the slant distance between the measured object and itself by calculating the time lag in phases or pulse timing. The horizontal distance and difference in elevation between each scanned cloud point and the measurement station can be further obtained by using the scanned horizontal and vertical direction angles.By this means the 3D relative coordinate differential between each scanned cloud point and the scanner can also be obtained. Coupled with different scanning angles, the 3D coordinate differentials from the scanner center to the measured point can be calculated while the magnitude of the response signals can be recorded simultaneously.

A time-of-flight (ToF) system measures range, ρ, by observing the two-way travel time, $\triangle$t, of a short (5-50ns in duration)(Amann et al. 2001) pulse of laser light,

$$\rho = \frac{1}{2} c\Delta t \tag{1}$$

Where c is the velocity of light and due to the reflective nature of the rangefinder there is no need to place retro-reflective targets on objects to be measured. Range to the surface is measured provided that a sufficient amount of pulse energy is reflected so as to register a signal with the photo-detector of the scanner. The current generated by the detector must exceed a predefined threshold in order for the return time to be observed.

The relative coordinates of 3D laser scanner are a local coordinate system formed with the laser source as the origin and scanning towards the right-hand side is is the X-axis direction while the direction facing the object is Y-axis and the vertical axis is Z direction. The distance and angle between the laser source

Table 1 The Trimble GS 200 LiDAR laser scanner specifications

Laser Wavelength	532 nm
Laser Class	class 3R
Scanning speed	Up to 10,000 points per second
Interface	Laptop/PDA(TCP/IP、Wireless、Wifi)
Field of view	Horizontal：360°(400g) Vertical：+30° to -30°
Standard range	2-200 m
Maximum range	350 m
Minimum resolution	3 mm at 100 m
Operating temperature	0℃ to 40℃
Accuracy	$1.4mm \pm D \times 10ppm$
Instrument weight	13.6 kg

Table 2 The RIEGL DIBIT LPM-2K LiDAR laser scanner specifications

Laser Wavelength	900 nm
Laser Class	class 3B
Scanning speed	4 points per second
Interface	Laptop(RS232 or RS432)
Field of view	Horizontal：360°(400 Gon) Vertical：+135° to -60°
Standard range	5-2000 m
Maximum range	up to 2500 m
Minimum resolution	15 mm at 100m
Operating temperature	0℃ to 50℃
Accuracy	$50mm \pm D \times 20ppm$
Instrument weight	14.6 kg

and the measured points are then calculated by the lags in timing and phases caused by emitting and receiving laser beams.

In Figure 3, SD is the calculated time difference between the laser distances. The degree of HA and VA is calculated from the inner-dial of the instrumentation. When applying, SD × *sin*(VA) = VD = Z and SD × *cos*(VA) = HD, HD × *sin*(HA) = X, HA × *cos*(HA) = Y the relative coordinate values of the X, Y, Z target points can be obtained.

4. Laser target

Different uses of laser scanners bring about different laser wavelengths or optical properties. Reflective laser targets are not necessarily manufactured the same, but are supposedly manufactured from strong laser reflective materials. The laser reflectors used as laser targets in this study have a diameter of 60mm.

The scanning mode during coordinate positioning by the instrumentation uses the reflective intensity value to ascertain the center point of the laser target. A software package is used to accurately undertake the scanning process. As the instrumentation will emit a laser beam, the reflected beam will be processed by the software where the reflected intensity and strength will be determined.

Using the coordinate conversion mathematical models, the conversion between the scanning space coordinates to object space coordinates can be represented by the following formulae, using three or more space control points in the conversion (Lichti et al. 2000).

$$\vec{R}_p = M\vec{r}_p + \vec{R}_s \tag{2}$$

$\vec{r}_p = [x_p \quad y_p \quad z_p]^T$: P point measured value in the scanning space coordinates.

$\vec{R}_p = [X_p \quad Y_p \quad Z_p]^T$: P point measured value in the object coordinates.

$\vec{R}_s = [X_s \quad Y_s \quad Z_s]^T$: Origin of scan coordinate at point S in the object space coordinate vector value。

The following three basic (gimbal-like) rotation matrices rotate vectors about the x, y, or z axis, in three dimensions:

$$R_x(\theta) = \begin{bmatrix} 1 & 0 & 0 \\ 0 & \cos\theta & -\sin\theta \\ 0 & \sin\theta & \cos\theta \end{bmatrix} \tag{3}$$

$$R_y(\theta) = \begin{bmatrix} \cos\theta & 0 & \sin\theta \\ 0 & 1 & 0 \\ -\sin\theta & 0 & \cos\theta \end{bmatrix} \tag{4}$$

$$R_z(\theta) = \begin{bmatrix} \cos\theta & -\sin\theta & 0 \\ \sin\theta & \cos\theta & 0 \\ 0 & 0 & 1 \end{bmatrix} \tag{5}$$

Rotation matrices can be obtained from these three using matrix multiplication. For example, the product $R_x(\omega)R_y(\varphi)R_z(\kappa)$ represents a rotation whose Euler angles are ω, φ, and κ. M is a matrix which around the (X、Y、Z) axis and rotation (ω、φ、κ) angle.

$$M = \begin{bmatrix} \cos\phi\cos k & \cos\omega\sin k + \sin\omega\sin\phi\cos k & \sin\omega\sin k + \cos\omega\sin\phi\cos k \\ -\cos\phi\sin k & \cos\omega\cos k - \sin\omega\sin\phi\sin k & \sin\omega\cos k + \cos\omega\sin\phi\sin k \\ \sin\phi & -\sin\omega\cos\phi & \cos\omega\cos\phi \end{bmatrix} \tag{6}$$

IV. SCANNING RESULTS

1. Scanning information

Intertidal scanning requires compliance with the tidal levels – with low tidal levels from 2009/03/01 to 2009/03/15 – a two week low tide period in which to undertaken the scanning process. In total, 56 scanning stations were present with 4 to 5 control points at each scanning station using VBS-RTK operations including control points measuring absolute coordinates. Using the VBS-RTK operations brings two advantages: firstly, scanning errors generated by the scanning stations can be controlled. Secondly, generated imagery from each scanning operation can be compiled into the same coordinate system. The scanning operation locations are denoted by red stars in Figure 4.

2. Information processing and accuracy

Cloud points from various scanning stations were combined with data from the ground control points. The conversion of the instrumentation coordinates and the actual space coordinates to a Taiwan coordinate system was undertaken using the Trimble Realworks Survey version 4.22 software package. Figure 5 shows the processed cloud point results. Towards the left of Figure 5 a coastal road can be clearly observed while on the right, the cloud points indicate the presence of a wave-and-tidal terrain.

Since each scanning station uses the VBS-RTK as control point measurements, each scanning station should have similar

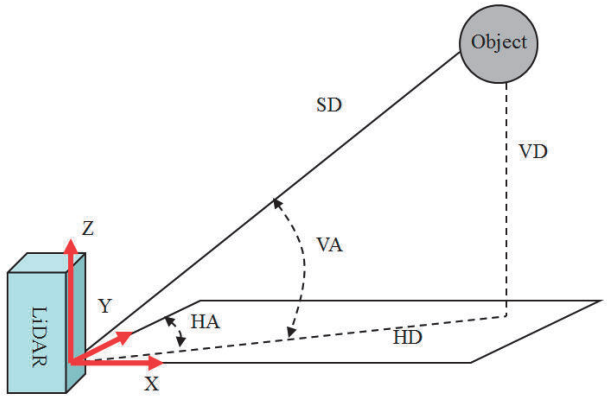

Fig.3 Diagram showing the relative coordinates between the object and the LiDAR

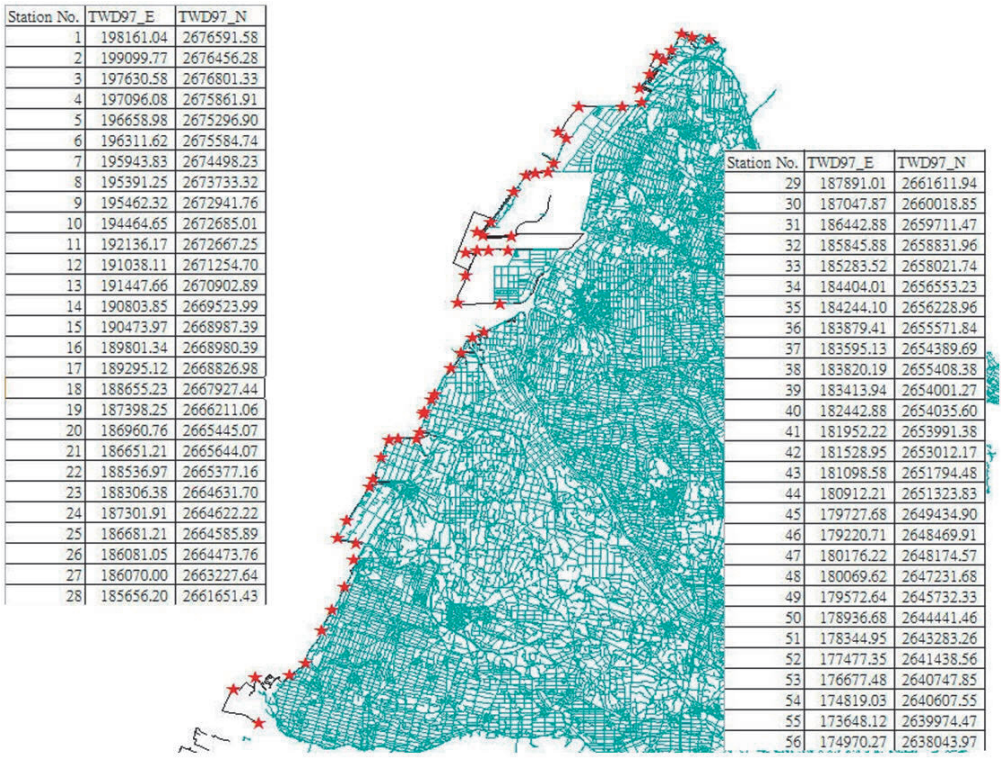

Station No.	TWD97_E	TWD97_N
1	198161.04	2676591.58
2	199099.77	2676456.28
3	197630.58	2676801.33
4	197096.08	2675861.91
5	196658.98	2675296.90
6	196311.62	2675584.74
7	195943.83	2674498.23
8	195391.25	2673733.32
9	195462.32	2672941.76
10	194464.65	2672685.01
11	192136.17	2672667.25
12	191038.11	2671254.70
13	191447.66	2670902.89
14	190803.85	2669523.99
15	190473.97	2668987.39
16	189801.34	2668980.39
17	189295.12	2668826.98
18	188655.23	2667927.44
19	187398.25	2666211.06
20	186960.76	2665445.07
21	186651.21	2665644.07
22	188536.97	2665377.16
23	188306.38	2664631.70
24	187301.91	2664622.22
25	186681.21	2664585.89
26	186081.05	2664473.76
27	186070.00	2663227.64
28	185656.20	2661651.43

Station No.	TWD97_E	TWD97_N
29	187891.01	2661611.94
30	187047.87	2660018.85
31	186442.88	2659711.47
32	185845.88	2658831.96
33	185283.52	2658021.74
34	184404.01	2656553.23
35	184244.10	2656228.96
36	183879.41	2655571.84
37	183595.13	2654389.69
38	183820.19	2655408.38
39	183413.94	2654001.27
40	182442.88	2654035.60
41	181952.22	2653991.38
42	181528.95	2653012.17
43	181098.58	2651794.48
44	180912.21	2651323.83
45	179727.68	2649434.90
46	179220.71	2648469.91
47	180176.22	2648174.57
48	180069.62	2647231.68
49	179572.64	2645732.33
50	178936.68	2644441.46
51	178344.95	2643283.26
52	177477.35	2641438.56
53	176677.48	2640747.85
54	174819.03	2640607.55
55	173648.12	2639974.47
56	174970.27	2638043.97

Fig.4 Diagram depicting the three dimensional Scanning locations within the Changhua coastline region.

Table 3 The accuracy of 56 scanning stations (Unit: mm)

Station number	Average accuracy	Vertical accuracy	Horizontal accuracy	Station number	Average accuracy	Vertical accuracy	Horizontal accuracy
1	20.3	16.425	11.929	29	18.6	17.280	6.882
2	18.5	14.505	11.482	30	19.3	17.826	7.398
3	17.8	14.330	10.558	31	17.8	17.624	2.494
4	22.2	18.609	12.105	32	23.4	22.739	5.522
5	20.4	17.456	10.557	33	18.9	15.450	10.886
6	17.6	17.414	2.553	34	20.1	16.154	11.961
7	18.3	14.294	11.427	35	20.7	18.507	9.272
8	21.7	21.575	2.326	36	19.9	17.434	9.596
9	17.2	13.973	10.030	37	20.7	17.812	10.546
10	22	21.103	6.217	38	16.7	16.643	1.383
11	23.7	22.874	6.203	39	16.8	12.242	11.506
12	16.9	13.762	9.809	40	17.4	16.547	5.381
13	16.7	13.685	9.571	41	23.7	21.780	9.345
14	22.6	19.875	10.758	42	19.2	15.957	10.677
15	21.9	18.375	11.915	43	22	20.946	6.726
16	19	18.296	5.124	44	19.5	17.984	7.538
17	18.9	17.211	7.809	45	19.7	19.497	2.824
18	16.9	13.402	10.296	46	21	17.681	11.330
19	19.5	16.196	10.861	47	19.4	16.278	10.554
20	19.9	16.531	11.079	48	19	18.578	3.983
21	20.4	18.823	7.864	49	21.1	21.090	0.659
22	19.3	17.118	8.914	50	17.5	17.046	3.961
23	21.6	20.896	5.469	51	20.8	18.582	9.346
24	17.9	13.054	12.247	52	20	19.397	4.875
25	18	17.408	4.578	53	19.3	17.291	8.574
26	19.4	17.841	7.621	54	20.7	18.181	9.896
27	20.1	16.250	11.830	55	18.7	17.674	6.108
28	18.8	17.017	7.992	56	16.9	16.417	4.012

accuracies in scanning values upon coordinate conversions. Typically the vertical accuracy will be 2 to 3 times worse than the horizontal accuracy. The accuracies from these operations are generally affected by the VBS-RTK with accuracies between 16mm to 24mm with an average accuracy of 19.57mm as shown in Table 3.

3. Data results

Upon completion of the operation, a total of 2,849,826 cloud points were collected. The shoreline and intertidal topography is shown as a cloud point form in Figure 6. The furthest detectable distance from the seawall was 2,587m, as depicted in Figure 6, with the deepest detectable depth at -0.5 elevation, shown in Figure 7. According to the tide gauge data from Central Weather Bureau (CWB), the test area lowest tide was -1.0m approximately during 2009 March. This can be observed in Figure 8. In Figure 9, a slightly shallower waterway can be observed which is the result of low tide. As residual seawater was still present, no cloud point data was collected.

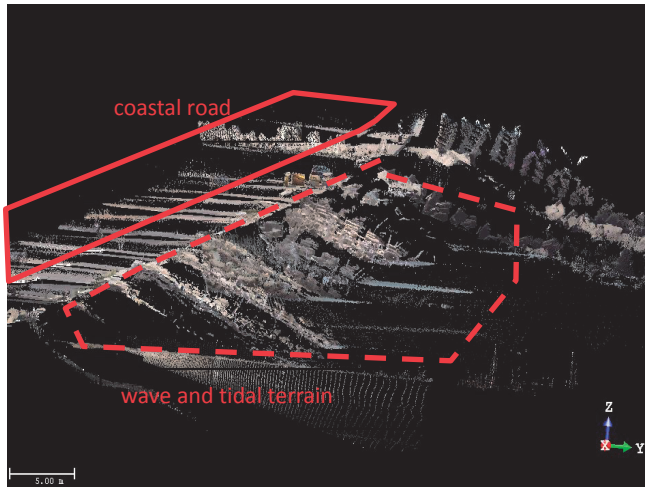

Fig.5 Screenshot of a resultant cloud point image – left side of the image shows a coastal road can be seen while on the right the wave and tidal terrain can be observed

Fig.6 Cloud point data results collected from the coast line with the furthest scan distance from the coast line at 2,587m

4. Extra applications

Using the cloud point data obtained in this operation, extra applications can be undertaken using software analysis. For example, contour lines can be quickly created as depicted in Figure 10. Figure 11 shows the possibility of generating topography and height profiles using software. The production of intertidal DTM data is also possible.

V. CONCLUSION

Previous intertidal measurements have been limited due to environmental and operational concerns. As such, true terrain and topography of such areas could not be determined. Recent years

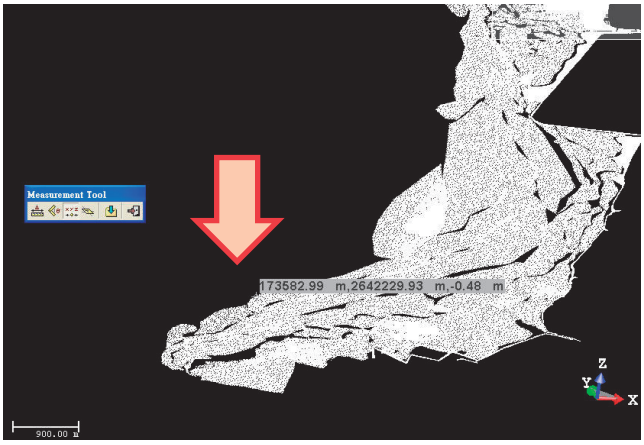

Fig.7 Deepest scanning depth at -0.48m elevation

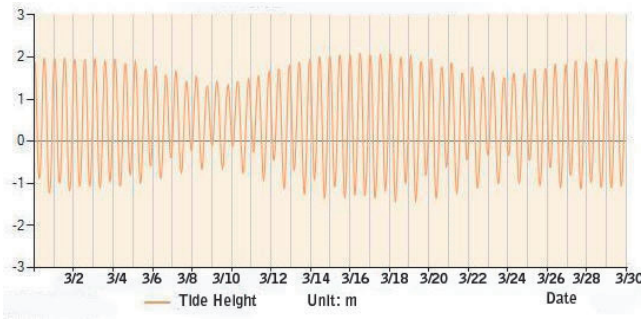

Fig.8 Tide gauge data from Central Weather Bureau during 2009 March.

Fig.9 Shallow water way can be observed after a low tide event

have seen the development of airborne LiDAR technology, However, its implementation may not necessarily be successful due to flight planning, costs and other considerations. This study attempts to use a ground-based LiDAR laser scanning system over an intertidal zone of up to 61km enabling a simple and fast method of determining intertidal topography. A total of 12 hours of 25 minutes is present between each low tidal event. Scans were completed during the low tidal periods with each measurement scans requiring two hours. The advantages of a ground-based laser system is the high-density cloud points and high precision features, the ability to process data immediately upon its collection and the ability to quickly identify the location of structures or water ways and in its accuracy in determining topographic changes.

1. Using the Ground-Based LiDAR with the addition of the VBS-RTK rapid dynamic positioning systems brings about 3 main advantages:
2. The measurement results can be converted into a local coordinate system.
3. Enabling each individual ground-based LiDAR to combine results.
4. Each individual Ground-Based LiDAR system with the addition of the VBS-RTK rapid dynamic positioning system has an error of between 16mm to 24mm. The accuracy is better than the airborne topographic LiDAR vertical accuracy of ±15cm and the airborne bathymetric LiDAR of ±1m (Quadros et al. 2008).

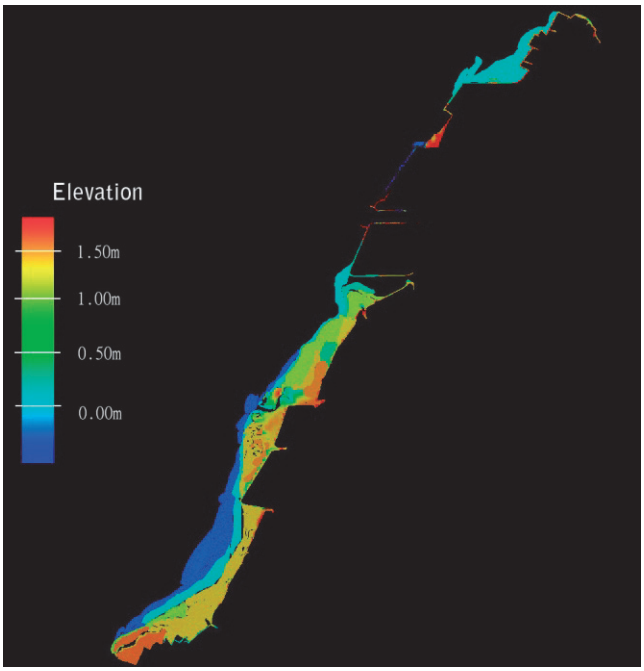

Fig.10 Using cloud points in creating topography maps

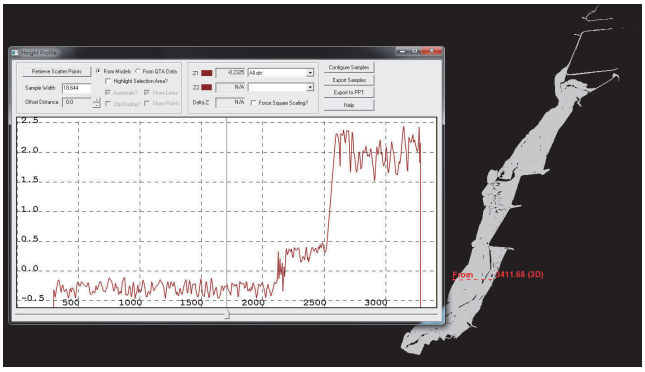

Fig.11 Generating intertidal topography and height profiles

This study was undertaken during the summer season due to its prolonged daylight hours. In some instances, two low tidal events would occur during daylight hours in one day (for example at 6am and 6pm), allowing for two measurement operations. Operations are limited during non-daylight hours. A scanning instrumentation with the longest scanning range of 2,500m was selected for this study. However upon a low tidal period, the sand slit can retract from the shore line by a distance of up to 5km. As such this study has not measured the complete intertidal area. In using a ground based laser system, an instrument or system with a larger scanning range would be required.

Ground based laser scanning systems require established control points. With the presence of GPS and IMU automobile-based mobile platform, scanning could be undertaken without the need for control point establishment.

References

[1] 儲慶美、簡裕城 (2004)。「GPS 新技術-虛擬參考站系統」，第六屆 GPS 衛星科技研討會論文集。(Chu, C.M., and Chien, Y.C. (2004). "The Virtual Base Station -GPS New Technology, taiwan." The Proceeding of the 6th Symposium on GPS Technology, Taiwan. (in Chinese))

[2] Amann, M.C., Bosch, T., Lescure, M., Myllyla, R., and Rioux, M. (2001). "Laser ranging: a critical review of usual techniques for distance measurement." Optical Engineering, 40(1), 10-19.

[3] Chen, M.C., Chen, C.S., Wu, C.T., and Edward, H. (2010). "Monitoring of Sag Deformation in Suspension Bridges using the 3D Laser Scanner." Materials Evaluation, 68(12), 1368-1378.

[4] Fang, H.M., Hsiao, S.S., Lai, C.T., and Cheng, G.L. "A Study of Using Kriging Method to Estimate the Topographic Data of Tideland." Proc., Proceedings of the 28th Ocean Engineering Conference in Taiwan, National Sun Yat-Sen University.

[5] Lichti, D.D., Stewart, M.P., Tsakiri, M., and Snow, A.J. (2000). "Calibration and Testing of A Terrestrial Laser Scanner." International Archives of Photogrammetry and Remote Sensing, Amsterdam.

[6] Matheron, G. (1963). "Principles of Geostatistics." Economic Geology, 58, 1246-1266.

[7] Quadros, N.D., Collier, P.A., and Fraser, C.S. (2008). "INTEGRATION OF BATHYMETRIC AND TOPOGRAPHIC LIDAR: A PRELIMINARY INVESTIGATION." The International Archives of the Photogrammetry, Remote Sensing and Spatial Information Sciences, Beijing, 1299-1304.

[8] Smart, G.M., Bind, J., and Duncan, M.J. (2009). "River bathymetry from conventional LiDAR using water surface returns." 18th World IMACS / MODSIM Congress, Australia.

[9] Wang, C.L., Hsiao, K.H., Yu, M.F., Cheng, D.K., and Liu, J.K. (2005). "Terrain Change Detection Using Airborne LiDAR Data." Ministry of the Interior conference, Taiwan, 237-246.

[10] Wang, M.S., Liu, C.C. and Lee, Y.H. (2006). "Setting A Real-Time Kinametic (RTK) System of National e-GPS Base Staions." M. o. I. National Land Surveying and Mapping Center, ed.

2012 年 08 月 13 日 收稿
2012 年 09 月 24 日 修正
2013 年 07 月 22 日 接受
(本文開放討論至 2014 年 9 月 30 日)